Finite-Element Model for Composite Beams with Arbitrary Cross-Sectional Warping

Alan D. Stemple* and Sung W. Lee†
University of Maryland, College Park, Maryland

A finite-element formulation has been developed to take into account the warping effect of composite beams. This formulation is to be used to model combined bending, torsional, and extensional behavior of composite beams. The new approach can model thin-walled beams with complicated cross sections, tapers, and arbitrary planforms. The strain is assumed to vary linearly through the wall thickness. Warping effects are properly incorporated in the formulation by assuming small warping displacements superimposed over cross sections in the deformed configuration. Transverse shear deformations are included. Numerical tests of example problems demonstrate the validity and effectiveness of the present approach. Comparisons of the present formulation with a shell element formulation and an experimental observation show excellent agreement.

Nomenclature

$\boldsymbol{a}_1,\boldsymbol{a}_2,\boldsymbol{a}_3$ = reference orthogonal unit vectors in the undeformed configuration
$\boldsymbol{a}'_1,\boldsymbol{a}'_2,\boldsymbol{a}'_3$ = reference orthogonal unit vectors in the deformed configuration
$\boldsymbol{B}^G,\boldsymbol{B}$ = global and local strain-displacement matrices, respectively
$\boldsymbol{C}$ = elastic constant matrix for orthotropic material in principal material axis
$\bar{\boldsymbol{C}}$ = elastic constant matrix for orthotropic material in rotated axis
E_1,E_2,E_3 = elastic moduli
$\boldsymbol{E}^G$ = global strain vector
f = warping displacement normal to deformed cross section
$\boldsymbol{F}$ = global load vector
G_{12},G_{13},G_{23} = shear moduli
$\boldsymbol{i}_1,\boldsymbol{i}_2,\boldsymbol{i}_3$ = global orthogonal unit vectors
$\boldsymbol{J}$ = Jacobian matrix
$\boldsymbol{K}$ = global stiffness matrix
$\boldsymbol{M}$ = scaled bending moment per unit length
$\boldsymbol{N}$ = scaled in-plane force per unit length
N_i^1 = one-dimensional shape function at node i
N_j^2 = two-dimensional shape function at node j
$\boldsymbol{q}$ = nodal displacement vector
t = thickness
$\boldsymbol{T}$ = tensor transformation matrix
$\boldsymbol{T}_c$ = composite material rotation matrix
$\boldsymbol{U}$ = global displacement vector of a generic point
U,V,W = components of $\boldsymbol{U}$
$\boldsymbol{X}$ = position vector of a generic point
X,Y,Z = components of $\boldsymbol{X}$
x_R,y_R,z_R = reference coordinates
$\boldsymbol{\varepsilon}$ = strain vector in local coordinate system
$\boldsymbol{\varepsilon}_m$ = strain vector in principal material system
$\boldsymbol{\varepsilon}^0$ = strain vector at midsurface
ε,η,ζ = nondimensional local coordinates
θ = angle between local axis and principal material axis
$\theta_1,\theta_2,\theta_3$ = rotations about reference axis x_R,y_R,z_R, respectively
$\boldsymbol{\kappa}$ = normalized strain curvature vector
$\nu_{12},\nu_{13},\nu_{23}$ = independent Poisson's ratios
$\boldsymbol{\sigma}$ = stress vector in local coordinate system
$\boldsymbol{\sigma}_m$ = stress vector in principal material system

Presented in part as Paper 87-0773 at the AIAA 28th Structures, Structural Dynamics, and Materials Conference, Monterey, CA, April 6–8, 1987; received July 23, 1987; revision received Dec. 14, 1987.

*Rotorcraft Fellow, Department of Aerospace Engineering.
†Associate Professor, Department of Aerospace Engineering.

I. Introduction

In today's aerospace industry the use of composite materials is becoming important due to the potential for saving weight, increasing fatigue life, and designing with aeroelastic tailoring. In general, composite materials cause a structure to be anisotropic and add complexity to the structural analysis.

Certain structural elements such as spars and helicopter blades can be approximated as beams, often with complicated cross-sectional geometries. They may be subject to combined axial, bending, and torsional loading.

In order to achieve maximum structural efficiency through aeroelastic tailoring, it is necessary to use composite laminates with different ply angles. As a result, composite beams will exhibit coupling among extensional stiffness, bending stiffness, and torsional stiffness. For example, extensional-torsional stiffness coupling is desirable to change the twist distribution for a two-speed rotor, and bending-torsional stiffness coupling is necessary for pitch-flap stability of helicopter rotor blades. Coupling between extension and torsion exists even for pretwisted isotropic beams.[1–3]

When warping is not present, the two most common beam theories are the Euler-Bernoulli theory and the shear-flexible theory. Unlike the Euler-Bernoulli theory, the shear-flexible theory allows transverse shear deformation. In shear-flexible theory the rotation variables are defined independently of translational displacements. This allows easy modeling of large deflections or finite rotations. Many finite-element formulations have been developed using these two theories without including the effect of warping.

Analytical and finite-element formulations exist that account for cross-sectional warping. For examples relevant to composite beams, see Refs. 4–8. However, these existing formulations do not allow for arbitrary warping and cannot accurately model the warping of complicated cross sections. Recently, Lee and Kim[9] developed a finite-element formulation that allows arbitrary warping for isotropic beams of complicated cross section, taper, and twist. In their formulation, a shear-flexible beam is used with a small warping displacement superimposed over the cross sections in the deformed configuration.

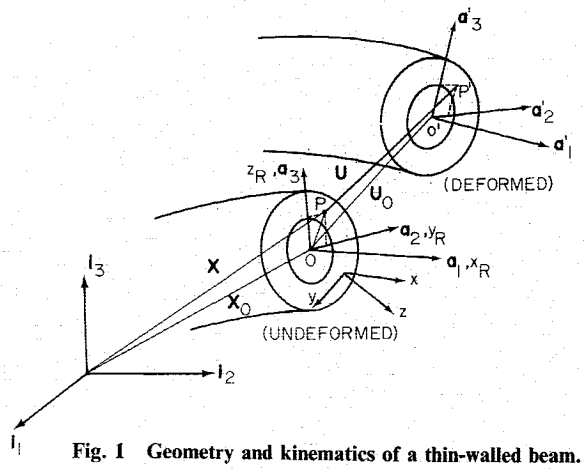

Fig. 1 Geometry and kinematics of a thin-walled beam.

In the present paper, the approach taken in Ref. 9 is extended to finite-element modeling of thin-walled composite beams. Again, the formulation adopts the shear-flexible beam theory and allows arbitrary cross-sectional warping. Although the formulation could be modified to allow for any type of polynomial strain distribution through the thickness, the formulation presented in this paper addresses thin-walled composite beams and thus assumes a linear strain distribution through the thickness.

In the present paper, the displacements are assumed small. A description of the kinematics of deformation, stress-strain relation, and formulation of the stiffness matrix is presented in the following sections. Subsequently, numerical tests are presented to validate the present approach.

II. Kinematics of Deformation

Figure 1 shows a part of a thin-walled beam before and after deformation. In the undeformed state, the generic material point p is in the plane normal to the beam axis at point 0. For the description of geometry and kinematics of deformation, a fixed global Cartesian coordinate system is defined with unit vectors $\boldsymbol{i}_1$, $\boldsymbol{i}_2$, and $\boldsymbol{i}_3$. For convenience, a reference coordinate system with components x_R, y_R, and z_R is defined such that the unit vector $\boldsymbol{a}_1$ is along the beam axis that is normal to the undeformed cross section. The unit vectors $\boldsymbol{a}_2$ and $\boldsymbol{a}_3$ are in the undeformed cross section such that together with $\boldsymbol{a}_1$ they form an orthogonal coordinate system. In addition, a local orthogonal coordinate system is set up on the midsurface of the wall such that the x axis is parallel to $\boldsymbol{a}_1$, the y axis is tangent to the wall midsurface, and the z axis is normal to the wall midsurface. With the above definitions of the coordinate systems, the position vector of point p before deformation can be expressed as

$$\boldsymbol{X} = \boldsymbol{X}_0 + y_R \boldsymbol{a}_2 + z_R \boldsymbol{a}_3 \tag{1}$$

where $\boldsymbol{X}$ is the position vector of point p with components X, Y, and Z in the global coordinate system, and $\boldsymbol{X}_0$ is the position vector of the point 0 with components in the global coordinate system.

Introducing one-dimensional shape functions $N_i^1(\xi)$, Eq. (1) can be expressed as

$$\boldsymbol{X} = \sum_{i=1}^{n} N_i^1 \boldsymbol{X}_0^i + \sum_{i=1}^{n} y_R^i N_i^1 \boldsymbol{a}_2^i + \sum_{i=1}^{n} z_R^i N_i^1 \boldsymbol{a}_3^i \tag{2}$$

where n is the number of nodes being considered for the one-dimensional shape function, and N_i^1 is the one-dimensional shape function for node i in terms of the nondimensional parent coordinate ξ. The quantities with superscript i are those evaluated at node i. For example, see Fig. 2a for the nodes located along the beam axis or x_R axis.

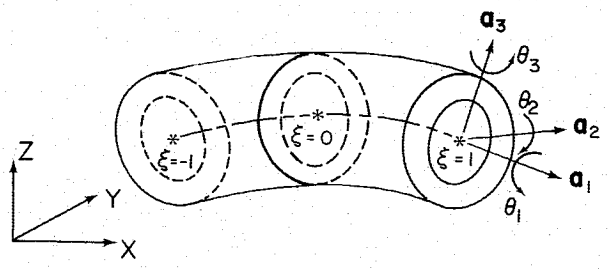

Fig. 2a Translation and rotation nodes of an element.

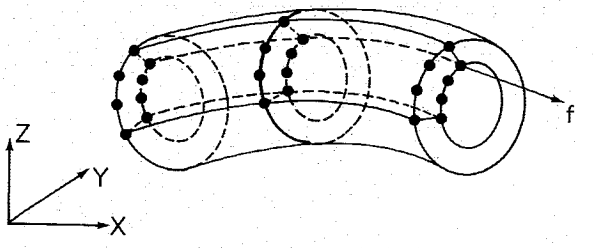

Fig. 2b Warping nodes of an element.

Over the cross section located at node i along the x_R axis, the coordinates y_R^i and z_R^i can be expressed in terms of nodal coordinates as

$$y_R^i = \sum_{j=1}^{m} N_j^2(y_R)_j^i \tag{3a}$$

$$z_R^i = \sum_{j=1}^{m} N_j^2(z_R)_j^i \tag{3b}$$

In Eq. (3), m is the number of nodes, $N_j^2(\eta,\zeta)$ is the two-dimensional shape function of the parent coordinates η and ζ, while the superscript i indicates the cross section located at node i along the x_R axis. See Fig. 2b for the nodes used to describe y_R^i and z_R^i.

A flat cross section that is initially normal to the beam axis or $\boldsymbol{a}_1$ translates and rotates in three-dimensional space. The unit vectors in the deformed configuration are defined as $\boldsymbol{a}_1'$, $\boldsymbol{a}_2'$, and $\boldsymbol{a}_3'$ as shown in Fig. 1. Small warping displacements are then superimposed over the flat cross section in the deformed configuration. The displacement vector $\boldsymbol{U}$ of a generic point p can be expressed as

$$\boldsymbol{U} = \boldsymbol{U}_b + \boldsymbol{U}_f \tag{4}$$

where $\boldsymbol{U}_b$ is the displacement associated with the three translational displacements and three rotational angles, and $\boldsymbol{U}_f$ is the warping displacement with one-dimensional component f in the direction normal to the cross section in the deformed configuration. If θ_1, θ_2, and θ_3 are rotation angles of the cross section around the $\boldsymbol{a}_1$, $\boldsymbol{a}_2$, and $\boldsymbol{a}_3$ axes, respectively, then for small angles the displacement vectors can be written as

$$\boldsymbol{U}_b = \boldsymbol{U}_0 + y_R(\theta_1 \boldsymbol{a}_3 - \theta_3 \boldsymbol{a}_1) + z_R(\theta_2 \boldsymbol{a}_1 - \theta_1 \boldsymbol{a}_2) \tag{5a}$$

$$\boldsymbol{U}_f = f\boldsymbol{a}_1 \tag{5b}$$

After introducing shape functions, the above equations may be written as

$$\boldsymbol{U}_b = \sum_{i=1}^{n} N_i^1 \boldsymbol{U}_0^i + \sum_{i=1}^{n}\sum_{j=1}^{m} N_j^2(y_R)_j^i N_i^1(\theta_1^i \boldsymbol{a}_3^i - \theta_3^i \boldsymbol{a}_1^i) + \sum_{i=1}^{n}\sum_{j=1}^{m} N_j^2(z_R)_j^i N_i^1(\theta_2^i \boldsymbol{a}_1^i - \theta_1^i \boldsymbol{a}_2^i) \tag{6}$$

$$U_f = \sum_{i=1}^{n} \sum_{j=1}^{m} N_j^2 f_j^i N_1^i a_1^i \tag{7}$$

where U_0^i, θ_1^i, θ_2^i, θ_3^i, and f_j^i are nodal values. It should be noted that over the cross section located at node i along the beam axis, the vector a_1^i is constant. Also, note that the assumed warping displacement vector U_f in Eq. (7) contains redundant rigid-body translations and rotations that must be suppressed.[9] This point will be discussed in Sec. V.

III. Strain Displacement Relation

Strain components corresponding to Eqs. (6) and (7) can be expressed in the global coordinate system or in the local coordinate system. For finite-element formulation, the strain components with respect to a particular coordinate system are expressed in terms of nodal degrees of freedom (DOF). For a beam with curved geometry and a complicated cross section, it is convenient to use strain in the local orthogonal coordinate system. In the present formulation, strain is initially expressed in the global coordinate system and then transformed to the local coordinate system through the strain transformation matrix.

For small deflection, the strain vector E^G in the global coordinate system, which has six components, can be expressed as

$$E^G = E_b^G + E_f^G \tag{8}$$

The global strain vector E_b^G corresponding to U_b can be expressed in terms of nodal displacements by

$$E_b^G = B_b^G(\xi,\eta,\zeta) q_b \tag{9}$$

where B_b^G is the global strain-displacement matrix and is a function of ξ, η, and ζ. The nodal displacement vector q_b is expressed by

$$q_b = [U_0^1, V_0^1, W_0^1, \theta_1^1, \theta_2^1, \theta_3^1, U_0^2, \ldots \theta_2^n, \theta_3^n]^T \tag{10}$$

and U_0^i, V_0^i, W_0^i are the global coordinate components of the displacement vector U_0^i at node i. The angles $\theta_1^i, \theta_2^i, \theta_3^i$ are the rotations about the reference axes at node i (see Fig. 2a).

Similarly, the global strain vector E_f^G that corresponds to U_f is expressed in terms of the nodal warping displacements as

$$E_f^G = B_f^G(\xi,\eta,\zeta) q_f \tag{11}$$

where B_f^G is the global warping strain-displacement matrix. The nodal warping displacement vector q_f is expressed as

$$q_f = \lfloor f_1^1, f_2^1, f_3^1, \ldots f_j^i \ldots f_m^n \rfloor^T \tag{12}$$

and f_j^i is the displacement of warping node j at cross-section i.

The global strain vectors E_b^G and E_f^G are related to the corresponding local strain vectors through the strain transformation matrix T such that

$$\varepsilon_b = T E_b^G = B_b q_b \tag{13}$$

$$\varepsilon_f = T E_f^G = B_f q_f \tag{14}$$

where

$$B_b = T B_b^G$$

$$B_f = T B_f^G$$

The total strain vector ε can then be expressed in the local coordinate system by

$$\varepsilon = \varepsilon_b + \varepsilon_f = B_b q_b + B_f q_f \tag{15}$$

Note that the local strain vector ε has only three components: ε_{xx}, ε_{zx}, and ε_{xy}.

In the present paper, an element is assumed to have two nodes in the thickness direction for the description of geometry and cross-sectional warping, as shown in Fig. 2b, and the strain is considered linear through the element thickness. Using the nondimensional coordinate ζ, $(-1 \le \zeta \le 1)$, through the element thickness, the strain vector can be expressed as

$$\varepsilon = \varepsilon^0 + \zeta \kappa \tag{16a}$$

where

$$\varepsilon^0 = \tfrac{1}{2}(\varepsilon_a + \varepsilon_{-a}) \tag{16b}$$

$$\kappa = (1/2a)(\varepsilon_a - \varepsilon_{-a}) \tag{16c}$$

In Eqs. (16b) and (16c), ε_a and ε_{-a} are ε at $\zeta = a$ and $\zeta = -a$, respectively. Note that $a = \sqrt{3}/3$ in accordance with the two-point Gaussian quadrature rule. Using Eq. (15), the above relationships may be written as

$$\varepsilon^0 = \tfrac{1}{2}[(B_b)_a + (B_b)_{-a}] q_b + \tfrac{1}{2}[(B_f)_a + (B_f)_{-a}] q_f \tag{17a}$$

$$\kappa = (1/2a)[(B_b)_a - (B_b)_{-a}] q_b + (1/2a)[(B_f)_a - (B_f)_{-a}] q_f \tag{17b}$$

where $(B_b)_a$ and $(B_f)_a$ are the strain-displacement matrices evaluated at the point $\zeta = a$, $(B_b)_{-a}$, and $(B_f)_{-a}$ are the strain-displacement matrices evaluated at the point $\zeta = -a$.

After rearranging, Eqs. (16b) and (16c) become

$$\begin{Bmatrix} \varepsilon^0 \\ \kappa \end{Bmatrix} = \begin{Bmatrix} B_{b\varepsilon} \\ B_{b\kappa} \end{Bmatrix} \{q_b\} + \begin{Bmatrix} B_{f\varepsilon} \\ B_{f\kappa} \end{Bmatrix} \{q_f\} \tag{18}$$

where

$$B_{b\varepsilon} = (1/2)[(B_b)_a + (B_b)_{-a}]$$

$$B_{b\kappa} = (1/2a)[(B_b)_a - (B_b)_{-a}]$$

$$B_{f\varepsilon} = (1/2)[(B_f)_a + (B_f)_{-a}]$$

$$B_{f\kappa} = (1/2a)[(B_f)_a - (B_f)_{-a}]$$

The $B_{b\varepsilon}$, $B_{b\kappa}$, $B_{f\varepsilon}$, and $B_{f\kappa}$ matrices are independent of ζ. Similarly, the determinant J of the Jacobian matrix J corresponding to Eq. (2) can be expressed as

$$J = J_0 + \zeta J_1 = J_0(1 + \alpha\zeta) \tag{19}$$

where

$$J_0 = (1/2)(J_a + J_{-a})$$

$$J_1 = (1/2a)(J_a - J_{-a})$$

$$\alpha = J_1/J_0$$

Again, J_a and J_{-a} are J evaluated at $\zeta = a$ and $\zeta = -a$, respectively.

IV. Stress-Strain Relation

Figure 3 shows a single-layer fiber-reinforced orthotropic composite lamina along with the two orthogonal coordinate systems used to describe it. The x,y,z system corresponds to the local coordinate system. For the 1,2,3, or principal material system, the 1 and 2 axes are embedded in the plane of the lamina with the 1 axis along the fiber direction and the 2 axis normal to the fiber direction. The 3 axis is identical to the z axis. For an orthotropic material, the linearly elastic stress-

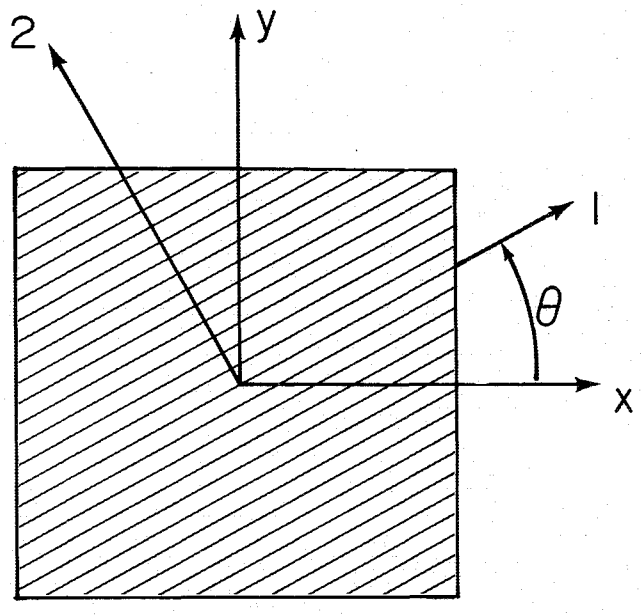

Fig. 3 Coordinate systems of a fiber-reinforced lamina.

strain relation is

$$\boldsymbol{\sigma}_m = \boldsymbol{C}\boldsymbol{\varepsilon}_m \tag{20}$$

where

$$\boldsymbol{\sigma}_m = [\sigma_{11}\sigma_{22}\sigma_{33}\sigma_{23}\sigma_{31}\sigma_{12}]^T$$

$$\boldsymbol{\varepsilon}_m = [\varepsilon_{11}\varepsilon_{22}\varepsilon_{33}\varepsilon_{23}\varepsilon_{31}\varepsilon_{12}]^T$$

and $\boldsymbol{C}$ is the 6×6 symmetric elastic constant matrix with the following nonzero entries:

$$C_{11} = (1 - \nu_{23}\nu_{32})E_1/\Lambda$$

$$C_{12} = C_{21} = (\nu_{12} + \nu_{13}\nu_{32})E_2/\Lambda$$

$$C_{13} = C_{31} = (\nu_{13} + \nu_{12}\nu_{23})E_3/\Lambda$$

$$C_{22} = (1 - \nu_{31}\nu_{13})E_2/\Lambda$$

$$C_{23} = C_{32} = (\nu_{23} + \nu_{21}\nu_{13})E_3/\Lambda$$

$$C_{33} = (1 - \nu_{21}\nu_{12})E_3/\Lambda$$

$$C_{44} = G_{23}, \qquad C_{55} = G_{31}, \qquad C_{66} = G_{12}$$

with

$$\Lambda = (1 - \nu_{12}\nu_{21} - \nu_{32}\nu_{23} - \nu_{13}\nu_{31} - 2\nu_{21}\nu_{13}\nu_{32})$$

All other entries are zero. The subscript m represents the principal material coordinate system. The stress vector $\boldsymbol{\sigma}$ and the strain vector $\boldsymbol{\varepsilon}$ in the x,y,z system are related to $\boldsymbol{\sigma}_m$ and $\boldsymbol{\varepsilon}_m$ through the transformation matrix T_c such that

$$\boldsymbol{\sigma} = \boldsymbol{T}_c\boldsymbol{\sigma}_m \tag{21a}$$

$$\boldsymbol{\varepsilon}_m = \boldsymbol{T}_c^T\boldsymbol{\varepsilon} \tag{21b}$$

Then for stress $\boldsymbol{\sigma}$ and strain $\boldsymbol{\varepsilon}$ in the x,y,z system

$$\boldsymbol{\sigma} = \bar{\boldsymbol{C}}\boldsymbol{\varepsilon} \tag{22}$$

where

$$\bar{\boldsymbol{C}} = \boldsymbol{T}_c\boldsymbol{C}\boldsymbol{T}_c^T$$

Introducing Eq. (16a) into Eq. (22),

$$\boldsymbol{\sigma} = \bar{\boldsymbol{C}}(\boldsymbol{\varepsilon}^0 + \zeta\boldsymbol{\kappa}) \tag{23}$$

The equations for $\boldsymbol{\sigma}$ and $\zeta\boldsymbol{\sigma}$ are then integrated over ζ to produce the following relationship:

$$\int_{-1}^{1} \begin{Bmatrix} \boldsymbol{\sigma} \\ \zeta\boldsymbol{\sigma} \end{Bmatrix}(1 + \alpha\zeta)\, d\zeta = \boldsymbol{P}\begin{Bmatrix} \boldsymbol{\varepsilon}^0 \\ \boldsymbol{\kappa} \end{Bmatrix} \tag{24}$$

where

$$\boldsymbol{P} = \int_{-1}^{1} \begin{bmatrix} \bar{\boldsymbol{C}} & \zeta\bar{\boldsymbol{C}} \\ \zeta\bar{\boldsymbol{C}} & \zeta^2\bar{\boldsymbol{C}} \end{bmatrix}(1 + \alpha\zeta)\, d\zeta$$

is a 12×12 symmetric matrix. Inverting Eq. (24) for a given α

$$\begin{Bmatrix} \boldsymbol{\varepsilon}^0 \\ \boldsymbol{\kappa} \end{Bmatrix} = \boldsymbol{P}^{-1}\int_{-1}^{1} \begin{Bmatrix} \boldsymbol{\sigma} \\ \zeta\boldsymbol{\sigma} \end{Bmatrix}(1 + \alpha\zeta)\, d\zeta \tag{25}$$

In accordance with the shear flexible beam theory, the following constraints now can be introduced into Eq. (25).

$$\int_{-1}^{1} \sigma_{yy}\, d\zeta = \int_{-1}^{1} \sigma_{zz}\, d\zeta = \int_{-1}^{1} \sigma_{yz} = 0 \tag{26a}$$

$$\int_{-1}^{1} \zeta\sigma_{yy}\, d\zeta = \int_{-1}^{1} \zeta\sigma_{zz}\, d\zeta = \int_{-1}^{1} \zeta\sigma_{yz}\, d\zeta = 0 \tag{26b}$$

$$\int_{-1}^{1} \zeta^2\sigma_{yy}\, d\zeta = \int_{-1}^{1} \zeta^2\sigma_{zz}\, d\zeta = \int_{-1}^{1} \zeta^2\sigma_{yz}\, d\zeta = 0 \tag{26c}$$

The constraints in Eqs. (26) reflect the assumption that the effect of the integrals on strain is negligible. When the rows corresponding to ε^0_{yy}, ε^0_{zz}, ε^0_{zy}, κ_{yy}, κ_{zz}, and κ_{yz} are deleted, $\boldsymbol{P}^{-1}$ reduces to a 6×6 matrix. The inverse of Eq. (25) is taken to give the following relationship:

$$\begin{Bmatrix} \boldsymbol{N} \\ \boldsymbol{M} \end{Bmatrix} = \begin{bmatrix} \boldsymbol{A} & \boldsymbol{B} \\ \boldsymbol{B}^T & \boldsymbol{D} \end{bmatrix}\begin{Bmatrix} \boldsymbol{\varepsilon}^0 \\ \boldsymbol{\kappa} \end{Bmatrix} \tag{27a}$$

where

$$\boldsymbol{N} = \begin{Bmatrix} N_{xx} \\ N_{zx} \\ N_{xy} \end{Bmatrix} = \begin{Bmatrix} \int_{-1}^{1} \sigma_{xx}(1 + \alpha\zeta)\, d\zeta \\ \int_{-1}^{1} \sigma_{zx}(1 + \alpha\zeta)\, d\zeta \\ \int_{-1}^{1} \sigma_{xy}(1 + \alpha\zeta)\, d\zeta \end{Bmatrix}, \qquad \boldsymbol{\varepsilon}^0 = \begin{Bmatrix} \varepsilon^0_{xx} \\ \varepsilon^0_{zx} \\ \varepsilon^0_{xy} \end{Bmatrix}$$

$$\boldsymbol{M} = \begin{Bmatrix} M_{xx} \\ M_{zx} \\ M_{xy} \end{Bmatrix} = \begin{Bmatrix} \int_{-1}^{1} \zeta\sigma_{xx}(1 + \alpha\zeta)\, d\zeta \\ \int_{-1}^{1} \zeta\sigma_{zx}(1 + \alpha\zeta)\, d\zeta \\ \int_{-1}^{1} \zeta\sigma_{xy}(1 + \alpha\zeta)\, d\zeta \end{Bmatrix}, \qquad \boldsymbol{\kappa} = \begin{Bmatrix} \kappa_{xx} \\ \kappa_{zx} \\ \kappa_{xy} \end{Bmatrix} \tag{27b}$$

In Eqs. (27), $\boldsymbol{A}$ represents in-plane stiffness, $\boldsymbol{B}$ represents in-plane stiffness coupling with bending stiffness, and $\boldsymbol{D}$ represents bending stiffness. Equation (18) gives $\boldsymbol{\varepsilon}^0$ and $\boldsymbol{\kappa}$ in terms of nodal displacements. With Eq. (18) and Eqs. (26), the generalized stresses $\boldsymbol{N}$ and $\boldsymbol{M}$ are related to the nodal displacements. The next section uses these relations to form the stiffness matrix.

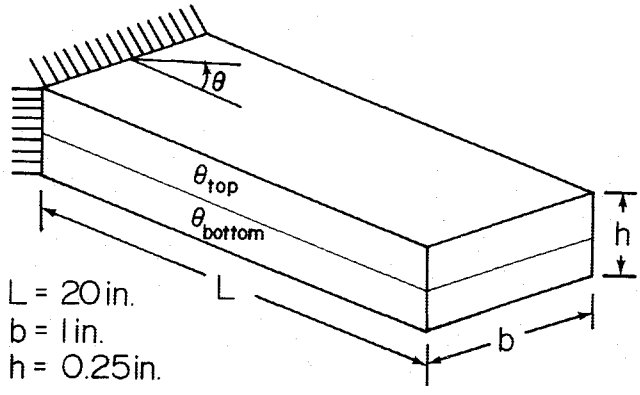

Fig. 4 Beam with solid rectangular cross section.

V. Formulation of Finite-Element Equation

A beam is initially divided into "translational and rotational" nodes and "warping" nodes. Figure 2 shows a typical element used in this paper. The element has three translational and rotational nodes, as shown in Fig. 2a, and 24 warping nodes, as shown in Fig. 2b. Each translational and rotational node has three translational DOF and three rotational DOF. Each warping node has a single DOF, which is normal to the deformed cross section.

For a solid body in equilibrium, the principle of virtual work states that

$$\delta\pi = \delta U - \delta W = 0 \tag{28a}$$

where

$$\delta U = \int_V \delta\boldsymbol{\varepsilon}^T\boldsymbol{\sigma}\,\mathrm{d}V \tag{28b}$$

is the internal virtual work, and δW is the external virtual work.

For an element, the internal virtual work δU_e can now be expressed as

$$\delta U_e = \int \delta\boldsymbol{\varepsilon}^T\boldsymbol{\sigma}\,\mathrm{d}V \tag{29}$$

Using the relationship in Eqs. (16a) and (19), δU_e becomes

$$\delta U_e = \int (\delta\boldsymbol{\varepsilon}^0 + \zeta\delta\boldsymbol{\kappa})^T\boldsymbol{\sigma}J_0(1+\alpha\zeta)\,\mathrm{d}\xi\,\mathrm{d}\eta\,\mathrm{d}\zeta \tag{30}$$

Equation (30) can be integrated through ζ such that

$$\delta U_e = \int (N_{xx}\delta\varepsilon^0_{xx} + N_{zx}\delta\varepsilon^0_{zx} + N_{xy}\delta\varepsilon^0_{xy} + M_{xx}\delta\kappa_{xx} + M_{zx}\delta\kappa_{zx} + M_{xy}\delta\kappa_{xy})J_0\,\mathrm{d}\xi\,\mathrm{d}\eta \tag{31a}$$

or

$$\delta U_e = \int \{\delta\boldsymbol{\varepsilon}^{0T}\delta\boldsymbol{\kappa}^T\}\begin{Bmatrix}\boldsymbol{N}\\ \boldsymbol{M}\end{Bmatrix}J_0\,\mathrm{d}\xi\,\mathrm{d}\eta \tag{31b}$$

Equation (31b) can be rewritten using the relation in Eq. (27a) as

$$\delta U_e = \int \{\delta\boldsymbol{\varepsilon}^{0T}\delta\boldsymbol{\kappa}^T\}\begin{bmatrix}\boldsymbol{A} & \boldsymbol{B}\\ \boldsymbol{B}^T & \boldsymbol{D}\end{bmatrix}\begin{Bmatrix}\boldsymbol{\varepsilon}^0\\ \boldsymbol{\kappa}\end{Bmatrix}J_0\,\mathrm{d}\xi\,\mathrm{d}\eta \tag{32}$$

From Eq. (18), $\boldsymbol{\varepsilon}^0$ and $\boldsymbol{\kappa}$ are known in terms of the nodal displacements. The element internal virtual work can now be written as

$$\delta U_e = \int_{-1}^{1}\left(\begin{Bmatrix}\boldsymbol{B}_{b\varepsilon}\\ \boldsymbol{B}_{b\kappa}\end{Bmatrix}\{\delta\boldsymbol{q}_b\} + \begin{Bmatrix}\boldsymbol{B}_{f\varepsilon}\\ \boldsymbol{B}_{f\kappa}\end{Bmatrix}\{\delta\boldsymbol{q}_f\}\right)^T \times\begin{bmatrix}\boldsymbol{A} & \boldsymbol{B}\\ \boldsymbol{B}^T & \boldsymbol{D}\end{bmatrix}\left(\begin{Bmatrix}\boldsymbol{B}_{b\varepsilon}\\ \boldsymbol{B}_{b\kappa}\end{Bmatrix}\{\boldsymbol{q}_b\} + \begin{Bmatrix}\boldsymbol{B}_{f\varepsilon}\\ \boldsymbol{B}_{f\kappa}\end{Bmatrix}\{\boldsymbol{q}_f\}\right)J_0\,\mathrm{d}\xi\,\mathrm{d}\eta \tag{33}$$

After rearranging, Eq. (33) becomes

$$\delta U_e = \delta\boldsymbol{q}_b^T\boldsymbol{K}_b\boldsymbol{q}_b + \delta\boldsymbol{q}_b^T\boldsymbol{K}_c\boldsymbol{q}_f + \delta\boldsymbol{q}_f^T\boldsymbol{K}_c^T\boldsymbol{q}_b + \delta\boldsymbol{q}_f^T\boldsymbol{K}_f\boldsymbol{q}_f \tag{34a}$$

where

$$\boldsymbol{K}_b = \int_{-1}^{1}\begin{Bmatrix}\boldsymbol{B}_{b\varepsilon}\\ \boldsymbol{B}_{b\kappa}\end{Bmatrix}^T\begin{bmatrix}\boldsymbol{A} & \boldsymbol{B}\\ \boldsymbol{B}^T & \boldsymbol{D}\end{bmatrix}\begin{Bmatrix}\boldsymbol{B}_{b\varepsilon}\\ \boldsymbol{B}_{b\kappa}\end{Bmatrix}J_0\,\mathrm{d}\xi\,\mathrm{d}\eta \tag{34b}$$

$$\boldsymbol{K}_c = \int_{-1}^{1}\begin{Bmatrix}\boldsymbol{B}_{b\varepsilon}\\ \boldsymbol{B}_{b\kappa}\end{Bmatrix}^T\begin{bmatrix}\boldsymbol{A} & \boldsymbol{B}\\ \boldsymbol{B}^T & \boldsymbol{D}\end{bmatrix}\begin{Bmatrix}\boldsymbol{B}_{f\varepsilon}\\ \boldsymbol{B}_{f\kappa}\end{Bmatrix}J_0\,\mathrm{d}\xi\,\mathrm{d}\eta \tag{34c}$$

$$\boldsymbol{K}_f = \int_{-1}^{1}\begin{Bmatrix}\boldsymbol{B}_{f\varepsilon}\\ \boldsymbol{B}_{f\kappa}\end{Bmatrix}^T\begin{bmatrix}\boldsymbol{A} & \boldsymbol{B}\\ \boldsymbol{B}^T & \boldsymbol{D}\end{bmatrix}\begin{Bmatrix}\boldsymbol{B}_{f\varepsilon}\\ \boldsymbol{B}_{f\kappa}\end{Bmatrix}J_0\,\mathrm{d}\xi\,\mathrm{d}\eta \tag{34d}$$

In the above equation, $\boldsymbol{K}_b$ represents the element stiffness matrix corresponding to the translational and rotational displacements $\boldsymbol{q}_b$, $\boldsymbol{K}_c$ is the element stiffness matrix due to the coupling between $\boldsymbol{q}_b$ and $\boldsymbol{q}_f$, and $\boldsymbol{K}_f$ represents the element stiffness matrix corresponding to the one-dimensional warping displacements $\boldsymbol{q}_f$.

Equation (34a) may be rewritten as

$$\delta U_e = \delta\boldsymbol{q}_e^T\boldsymbol{K}_e\boldsymbol{q}_e \tag{35}$$

where

$$\boldsymbol{K}_e = \begin{bmatrix}\boldsymbol{K}_b & \boldsymbol{K}_c\\ \boldsymbol{K}_c^T & \boldsymbol{K}_f\end{bmatrix} \tag{36}$$

is the element stiffness matrix and

$$\boldsymbol{q}_e = \begin{Bmatrix}\boldsymbol{q}_b\\ \boldsymbol{q}_f\end{Bmatrix} \tag{37}$$

is the element nodal displacement vector.

The global stiffness matrix is obtained by assembling the element stiffness matrices. As mentioned earlier, the superposition of warping displacement over translation and rotation of a cross section introduces redundant rigid-body translations and rotations. In order to eliminate the redundant rigid-body modes, three arbitrary warping displacements are fixed on each cross section.[9] This creates a flat surface, a reference plane from which warping displacements are measured.

The external virtual work δW_e for a single element can be expressed symbolically as

$$\delta W_e = \delta\boldsymbol{q}_e\boldsymbol{Q}_e^T \tag{38}$$

where $\boldsymbol{Q}_e$ is the element load vector. After the element stiffness matrices and element load vectors are assembled to give the global stiffness matrix $\boldsymbol{K}$ and the global load vector $\boldsymbol{F}$, the following equation

$$\boldsymbol{K}\boldsymbol{q} = \boldsymbol{F} \tag{39}$$

is solved for the nodal displacements.

VI. Numerical Tests and Discussion

To verify the usefulness of the new formulation presented in this paper, several numerical tests of various problems were performed. The results of the numerical tests are compared with an experimental result and other independent numerical

solutions using shell finite-element models. A hollow elliptical cross section and a hollow circular cross-section beam as well as a solid rectangular cross-section beam were chosen as example problems. Reference 9, which deals with isotropic beams, includes results of numerical tests for pretwisted and tapered beams.

All examples were calculated using double-precision accuracy on the University of Maryland's Sperry 1100/92 computer system. For convenience, the element mesh will be written as $q \times r$, where q represents the number of elements in the beam axis or longitudinal direction, and r represents the number of elements in the cross section.

Thin Rectangular Section

To examine the ability of the present finite-element model to handle the extensive stiffness coupling, a simple two-layer fiber-reinforced rectangular beam was considered. Figure 4 shows the cantilever beam with its dimensions. The material used is T300/5208 graphite/epoxy with the following properties:

$$E_1 = 21.3 \times 10^6 \text{ psi}$$

$$E_2 = E_3 = 1.6 \times 10^6 \text{ psi}$$

$$G_{12} = G_{13} = 0.9 \times 10^6 \text{ psi}$$

$$G_{23} = 0.7 \times 10^6 \text{ psi}$$

$$\nu_{12} = \nu_{13} = 0.28$$

$$\nu_{23} = 0.5$$

Two types of ply layups, $[\theta/0]$ and $[\theta/-\theta]$, were chosen with the angle θ varying from 0 to 90 deg. The separate effects of the following loadings, applied at the tip, were investigated: a unit longitudinal load, a unit shear or vertical load, and a unit torsional load.

Results using the present formulation are for a 2×1, 44 DOF element mesh. The nodal distribution of a cross section is shown in Fig. 5. Figures 6a–i show the results of the three applied loads on the beam. In addition, the converged solution for a finite-element code using a shell formulation[10,11] is also plotted in Figs. 6a–i for comparison. This example shows that the present formulation accurately models the coupling between bending, torsion, and extension. Considering the relative thickness of this specimen, a mesh with multiple elements in the thickness direction may be investigated.

Hollow Circular Section

The second structure modeled was an eight-layer fiber-reinforced composite beam with a hollow circular cross section. Figure 7 shows the geometric dimensions of the beam with $L = 24$ in., $R = 0.804$ in., and $t = 0.04$ in. The material used for the cylinder was T300/5208 as in the previous example, and the ply layup used was $[(-20/70)_2]_s$. The cylinder was subject to two loading conditions. First, a uniformly distributed longi-

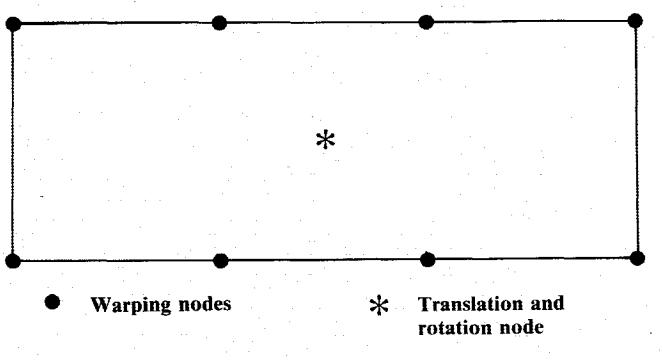

Fig. 5 Nodal distribution on rectangular cross section.

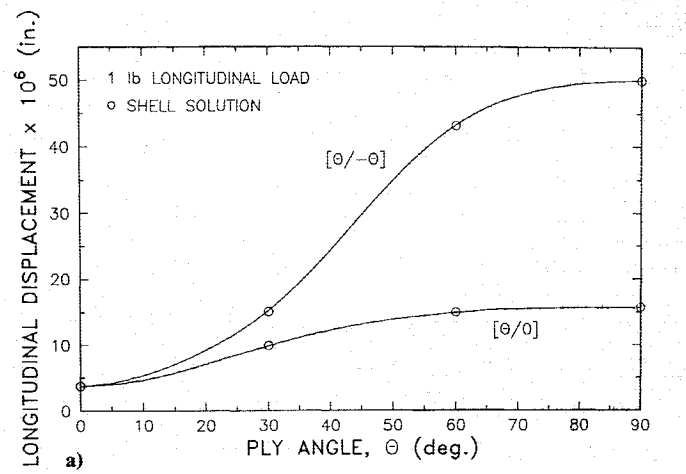

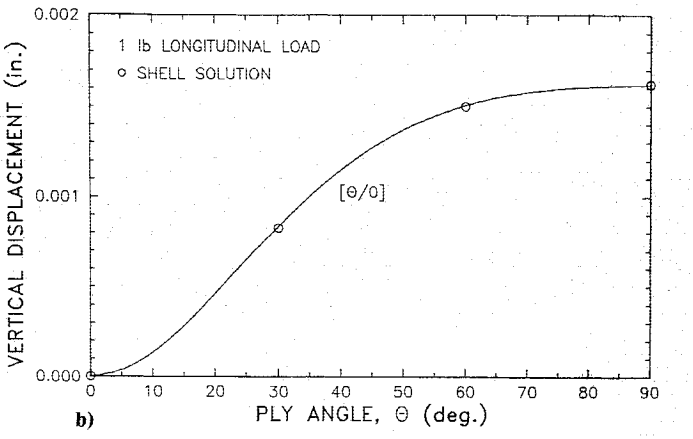

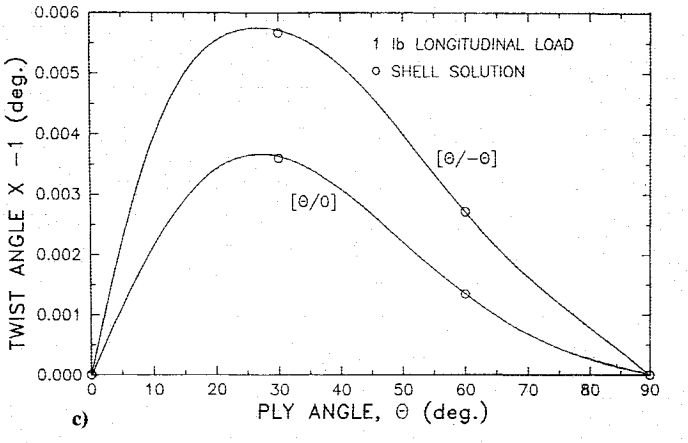

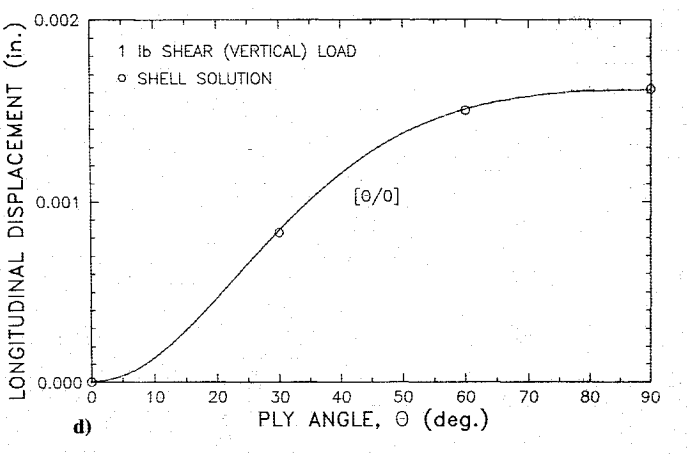

Fig. 6 Displacements of a two-layer rectangular section beam subject to a unit load.

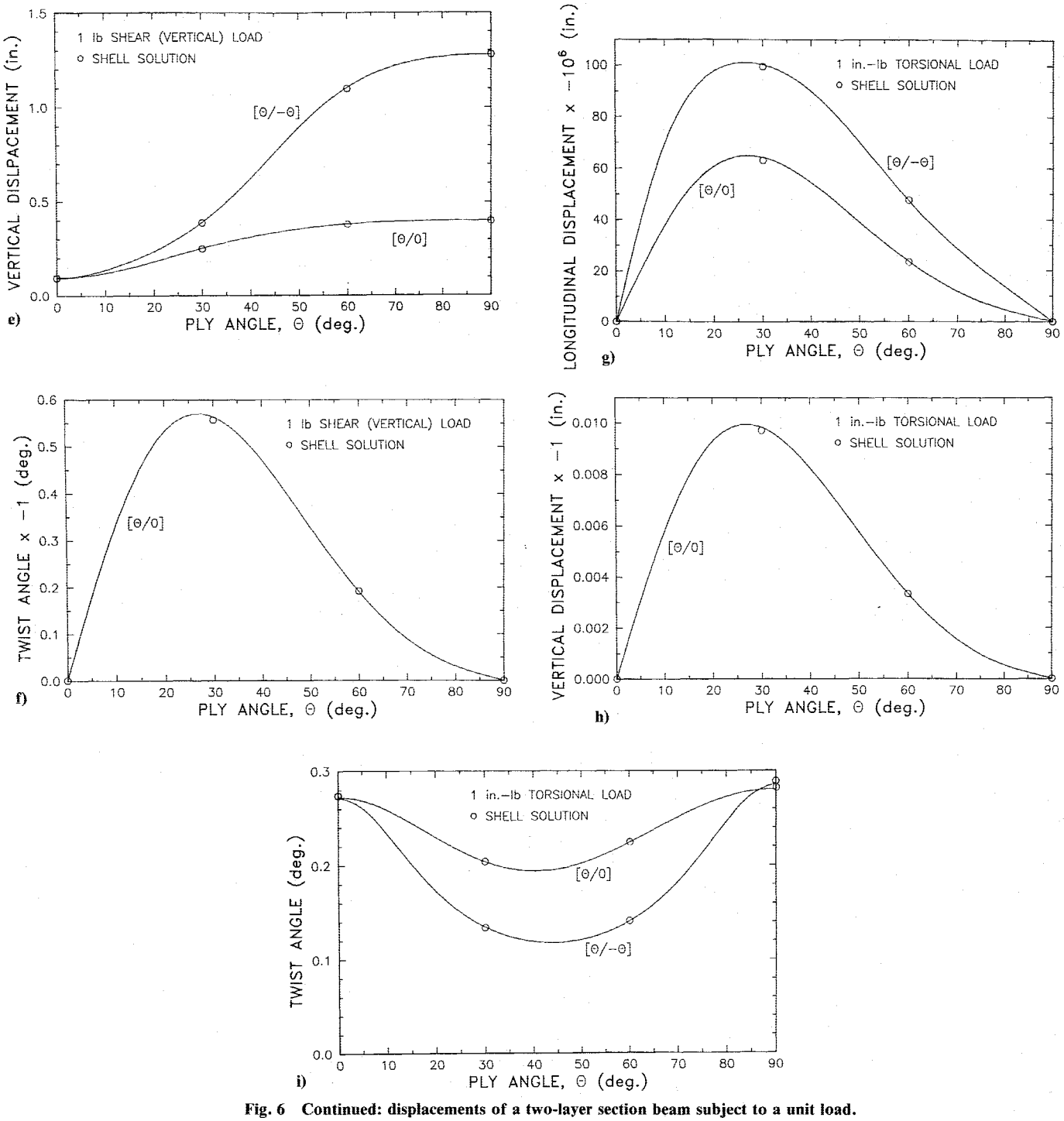

Fig. 6 Continued: displacements of a two-layer section beam subject to a unit load.

tudinal load of 1000 lb was applied at the tip to show the coupling between extension and twisting. Second, a shear load of 10 lb was applied at the tip. Four element meshes were used to verify convergence. The element meshes are 1×4, 1×8, 1×12, and 4×4. Figure 8 shows the nodal distribution of a cross section with four elements.

Table 1 contains the axial displacement and twist angle at the tip for the longitudinal loading condition and the tip deflections for the shear load. The converged solutions from a shell element formulation are also presented in Table 1. In addition, the experimental observation of Nixon[12] for an axial loading is included in Table 1. These results show excellent agreement. Because of the axisymmetry, there is no cross-sectional warping in this problem. However, the warping nodes are still needed to describe the geometry of the cross section. For the circular geometry used, eight elements per cross section gave convergence to four digits of accuracy. More complicated cross sections would require more elements to model the geometry and the cross-sectional warping accurately.

Hollow Elliptical Section

The third structure modeled was an eight-layer composite beam with a hollow elliptical section. The layup used was $[(-20/70)_2]_s$, the material used was T300/5208 as in the previous example. The cross-sectional dimensions are shown in Fig. 9 with $a = 20$ in., $b = 10$ in., and $t = 1.0$ in. The beam length was 1000 in. Three loading conditions were applied to the beam, each having a unit magnitude. In addition to the two types of loads applied to the circular cylinder, a torsional load was applied to the tip.

Table 2 shows the displacements predicted by the present formulation using a 1×12 mesh for the above loading condi-

Table 1 Composite circular cylinder under uniformly distributed tip axial and shear loads

	Longitudinal load (1000 lb)		Shear load (10 lb)
Element mesh	Twist angle θ_1 (deg)	Axial displacement $u \times 10^2$ (in.)	Tip displacement w (in.)
1×4	−1.9287	2.1676	0.12976
1×8	−1.9329	2.1708	0.13015
1×12	−1.9332	2.1710	0.13018
4×4	−1.9287	2.1676	0.12971
Shell element solution	−1.929	2.171	0.12978
Experimental observation	−1.98		

Table 2 Composite elliptical cylinder under unit tip loads

	Longitudinal load		Shear load	Torsion load
	Twist angle $\theta_1 \times 10^0$ (deg)	Axial displacement $u \times 10^6$ (in.)	Tip displacement w (in.)	Twist angle $\theta_1 \times 10^8$ (deg)
Present formulation	−10.429	1.888	0.010854	2.5494
Shell formulation	−10.419	1.887	0.010798	2.5446

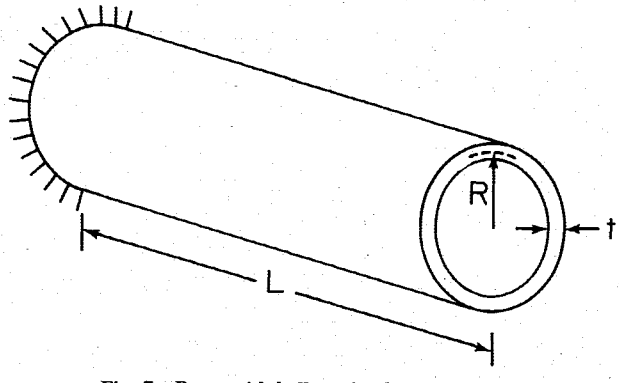

Fig. 7 Beam with hollow circular cross section.

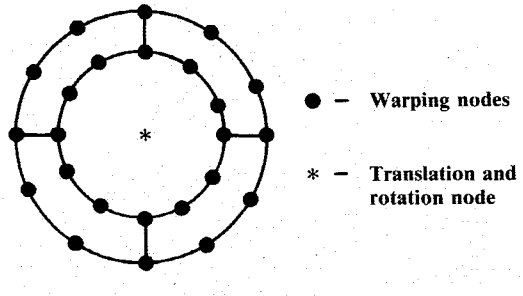

Fig. 8 Nodal distribution on the cross section of a circular cylinder with four elements.

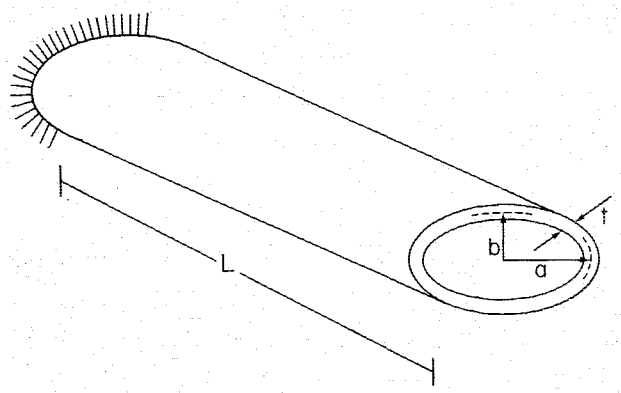

Fig. 9 Beam with hollow elliptical cross section.

tions. The converged solutions from a shell element formulation are also presented. The maximum differences between the two solutions are less than 0.6%.

VII. Conclusions

The results of the numerical tests presented in this paper show that the present formulation can model the extensive stiffness coupling found in composites. For the fiber-reinforced composite beams, results were compared to those from a shell element formulation. Good agreement was found between the two formulations. However, the beam model presented in this paper involves about 60% fewer total degrees of freedom than the shell element model. Accordingly, the beam model requires much less computing effort than the shell model. In addition, for rotor aeroelastic problems in which aerodynamics is coupled with structural stiffness, it is more convenient to model rotor blades as beams rather than as shells. In the case where an experimental result was available for the hollow circular cylinder under a longitudinal load, good agreement was observed. For the cases tested, the convergence characteristics were very good. The results for the test cases demonstrates the validity of the approach introduced in this paper to incorporate the warping effect properly.

Although rather simple geometries were presented in this paper, the formulation is applicable to complicated geometries. For cross sections with walls that cannot be considered thin, the present formulation should be modified to allow for a higher-order polynomial distribution of strain through the thickness. Extension to the modeling of large deflections or finite rotations for composite beams will be made in the near future.

References

[1]Rosen, A., "The Effect of Initial Twist on the Torsional Rigidity of Beams—Another Point of View," *ASME Journal of Applied Mechanics*, Vol. 47, June 1980, pp. 389–392.

[2]Hodges, D. H., "Torsion of Pretwisted Beams Due to Axial Loading," *ASME Journal of Applied Mechanics*, Vol. 47, June 1980, pp. 393–397.

[3]Krenk, S., "A Linear Theory for Pretwisted Elastic Beams," *ASME Journal of Applied Mechanics*, Vol. 50, March 1983, pp. 137–142.

[4]Bauchau, O. A., "A Beam Theory for Anisotropic Materials," *ASME Journal of Applied Mechanics*, Vol. 52, June 1985, pp. 416–422.

[5]Bauchau, O. A., Coffenberry, B. S., and Rehfield, L. W., "Composite Box Beam Analysis: Theory and Experiments," *Journal of Reinforced Plastics and Composites*, Vol. 6, Jan. 1987, pp. 25–35.

[6]Worndle, R., "Calculation of the Cross Section Properties and the Shear Stress of Composite Rotor Blades," *Vertica*, Vol. 6, No. 2, 1982, pp. 111–129.

[7]Mansfield, E. H. and Sobey, A. J., "The Fibre Composite Helicopter Blade," *Aeronautical Quarterly*, Vol. 30, No. 2, May 1979, pp. 413–449.

[8]Hong, C. H. and Chopra, I., "Aeroelastic Stability Analysis of a Composite Bearingless Rotor Blade," *Journal of the American Heli-*

copter Society, Vol. 31, No. 4, 1986, pp. 29–35.

[9]Lee, S. W. and Kim, Y. H., "A New Approach to the Finite Element Modeling of Beams with Warping Effect," *International Journal of Numerical Methods in Engineering*, Vol. 24, Dec. 1987, pp. 2327–2341.

[10]Lee, S. W., Wong, S. C., and Rhiu, J. J., "Study of A Nine-Node Mixed Formulation Finite Element for Thin Plates and Shells," *Computers and Structures*, Vol. 21, No. 6, 1985, pp. 1325–1334.

[11]Rhiu, J. J. and Lee, S. W., "A New Efficient Mixed Formulation for Thin Shell Finite Element Models," *International Journal of Numerical Methods in Engineering*, Vol. 24, No. 3, 1985, pp. 581–604.

[12]Nixon, M. W., "Extension-Twist Coupling of Composite Circular Tubes with Application to Tilt Rotor Design," Monterey, CA, AIAA Paper 87-0772, April 1987.